

# Imprints of the ejecta-companion interaction in Type Ia supernovae: main sequence, subgiant, and red giant companions

P. Boehner<sup>1\*</sup>, T. Plewa<sup>1\*</sup>, N. Langer<sup>2\*</sup>

<sup>1</sup>*Department of Scientific Computing, Florida State University, Tallahassee, FL 32306, U.S.A.,*

<sup>2</sup>*Argelander-Institut für Astronomie der Universität Bonn, Aufdem Hügel, D-53121 Bonn, Germany*

Accepted 2016 October 20. Received 2016 October 11; in original form 2016 August 17

## ABSTRACT

We study supernova ejecta-companion interactions in a sample of realistic semidetached binary systems representative of Type Ia supernova progenitor binaries in a single-degenerate scenario. We model the interaction process with the help of a high-resolution hydrodynamic code assuming cylindrical symmetry. We find that the ejecta hole has a half-opening angle of 40–50° with the density by a factor of 2–4 lower, in good agreement with the previous studies. Quantitative differences from the past results in the amounts and kinematics of the stripped companion material and levels of contamination of the companion with the ejecta material can be explained by different model assumptions and effects due to numerical diffusion. We analyse and, for the first time, provide simulation-based estimates of the amounts and of the thermal characteristics of the shock-heated material responsible for producing a prompt, soft X-ray emission. Besides the shocked ejecta material, considered in the original model by Kasen, we also account for the stripped, shock-heated envelope material of stellar companions, which we predict partially contributes to the prompt emission. The amount of the energy deposited in the envelope is comparable to the energy stored in the ejecta. The total energy budget available for the prompt emission is by a factor of about 2–4 smaller than originally predicted by Kasen. Although the shocked envelope has a higher characteristic temperature than the shocked ejecta, the temperature estimates of the shocked material are in good agreement with the Kasen’s model. The hottest shocked plasma is produced in the subgiant companion case.

**Key words:** hydrodynamics – instabilities – shock waves – binaries: close – supernovae: general

## 1 INTRODUCTION

Type Ia supernovae (SNeIa), are used as ‘standard candles’ to measure cosmological distances (Phillips 1993) and the expansion rate of the universe (Branch & Tammann 1992). However, the fundamental processes leading up to these events are still not fully understood (see, e.g. Hillebrandt & Niemeyer 2000, and references therein). Though much work has gone into improving the procedure used to standardize the SNIa light curves, this method is mainly empirical and does not take into account the physical properties of the exploding objects. It is conceivable that individual supernova events will be characterized with different energies and nucleosynthetic yields depending on the actual state of

the exploding object. In the Type Ia single degenerate (SD) scenario (Whelan & Iben 1973; Nomoto 1982), the explosion involves a massive white dwarf while in the double degenerate (DD) scenario (Iben & Tutukov 1984; Webbink 1984), two white dwarfs in a close binary system violently merge in a process that is expected to eventually produce an explosion.

Identifying which specific scenario produced a particular Type Ia supernova requires precise observations. For example, no companion star should be found near the center of the explosion site following the SNIa explosion in the binary white dwarf system. In contrast, one expects to observe a late-type star in the immediate vicinity of the Type Ia supernova produced in the SD channel. The observations of field stars in the central region of Tycho supernova remnant have provided the strongest evidence for such a late-type companion star (Ruiz-Lapuente et al. 2004; Ruiz-Lapuente

\* E-mail: philboehner@gmail.com (PB); tplewa@fsu.edu (TP); nlangier@astro.uni-bonn.de (NL)

2014), although the reported discovery remains controversial (Xue & Schaefer 2015; Williams et al. 2016). In addition, the imaging and spectroscopic observations of the remnant may provide evidence for interaction between the progenitor system with the interstellar medium (Zhou et al. 2016). Some theoretical models predict supernova ejecta to show morphological or compositional features that could be linked to the presence of a non-degenerate companion star (see, e.g. Marietta et al. 2000).

The process of the interaction between the supernova and a late-type stellar companion should also produce a substantial amount of shocked material, which could produce excess radiation in the UV and possibly also in the soft X-rays. Detection of such excess emission was recently reported in the Type Ia supernovae SN iPTF14atg (Cao et al. 2015) and SN 2012cg (Marion et al. 2016). The interpretation of the observed excess emission follows the theoretical model by Kasen (2010), who was the first to consider the emission produced in the process of collision between the Type Ia supernova ejecta with various non-degenerate stellar companions.

Such interactions were originally modeled by means of hydrodynamic simulations by Marietta et al. (2000). These authors performed the comprehensive study in two spatial dimensions using a high resolution finite volume hydrocode. They considered a variety of plausible single-degenerate progenitor systems with main sequence (MS), subgiant (SG), and red giant (RG) companions. They quantified the amount of hydrogen stripped from the companion, the velocity distribution of the stripped mass, the momentum transferred by the ejecta to the companion (the kick velocity), and the contamination of the companion with supernova ejecta material. Their most notable prediction was the existence of a low-density region carved in the ejecta by the companion. Since then, this specific morphological feature of a single-degenerate Type Ia supernova remnant is commonly known as the “ejecta hole”.

The results of Marietta et al. (2000) were later scrutinized in three dimensions by Pakmor et al. (2008). This group used a smoothed particle hydrodynamics (SPH) method and limited their studies to MS companions. They considered the dependence of model outcomes on the supernova explosion energy and the distance to the companion, and found evidence for a power-law relation between the amount of stripped mass and the kick velocity on the explosion energy based on the analysis of one of their model binary systems. Their findings in regard to the geometry of the ejecta hole largely confirmed the original predictions of Marietta et al. (2000).

More recently, Liu et al. (2012) further developed a SPH model of Pakmor et al. (2008) and used improved MS companion models obtained in the course of pre-supernova binary evolution Ivanova & Taam (2004). They found much higher amounts of material stripped from companions than reported by Pakmor et al. (2008). Additionally, they found that although the amount of stripped mass and kick velocity still depend on the impact geometry (the ratio between the stellar companion radius and the orbital separation), the actual relations also depend on the companion’s structure. These types of power law correlations, including the amount of contamination as a function of the explosion energy, were

later reported by Liu et al. (2013b) also in the case of a helium companion.

Pan et al. (2010) were the first to employ an adaptive mesh refinement technique to study the interaction process, and considered a binary system with a helium companion in two dimensions. They found power-law relations for the amount of stripped mass and kick velocity of the companion similar to those originally reported by Pakmor et al. (2008). Their model was later extended in Pan et al. (2012a), who accounted for the effects of orbital motion and the companion’s spin. In that more recent work, they performed an extensive parameter survey in two and three dimensions varying binary orbital separations for RG, MS, and helium companions. In regard to contamination of companion stars with the ejecta material, they found that the amount of contamination of their model MS companion was comparable to that reported by Marietta et al. (2000). However, in the case of a compact helium companion, the level of contamination was an order of magnitude greater than obtained by Marietta et al. (2000). Additionally, they found no substantial amount of supernova debris deposited onto their RG model companion.

The evolution of the companion star after the interaction with the supernova ejecta is addressed in more recent studies. For the short-term evolution of the surviving companion star, Liu et al. (2013a) studied MS companion stars in three dimensions for about 3 h, finding that the rotational velocity is reduced to about a fourth of the pre-supernova velocity due to expansion and the fact that much of the angular momentum was carried away by the stripped mass. For the long-term evolution, Pan et al. (2012b, 2013), using the methods and results of Pan et al. (2012a) as input for a one-dimensional stellar evolution code for MS, SG, and helium stars, found that the rotational velocity of the companion star will be reduced and the star will enter a highly luminous phase years following the supernova event. Pan et al. (2014) then found an upper limit in terms of detection for the distance a MS or helium star could travel after being kicked from the explosion site.

The long-term evolution of the ejecta hole was studied by García-Senz et al. (2012), using an SPH technique. They considered a single system with a main-sequence companion and accounted for the effects of orbital motion. They conjectured that the hole will likely close on the time scale of centuries due to hydrodynamic instabilities. It should be noted, however, that these authors did not consider the role of perturbations existing in the interstellar medium, such as turbulence, that would likely contribute to the destruction of the ejecta hole and mixing of the material stripped from the companion with the ejecta.

Our aim is to extend the above studies by performing hydrodynamic simulations of the supernova ejecta-companion interaction for a rich set of binary systems considered to be realistic progenitor systems of Type Ia supernovae in the single degenerate channel. We discuss a range of basic model outputs such as the structure of the ejecta hole, kinematic properties of the stripped companion material, and pollution of the supernova companion stars by the supernova ejecta, and compare them to the results obtained by other groups. More importantly, and in the context of the prompt soft X-ray emission model, we carefully analyze and, for the first time, provide information about the amounts

and thermal characteristics of the energy stored in the ejecta and in the envelope of the companion by shocks created due to collision between the ejecta on the companion's envelope. The contribution of the shocked envelope material to the prompt emission was not included in the original model by [Kasen \(2010\)](#). Our results provide input to more realistic radiative transport calculations of the prompt emission that should help discerning different types of companion stars using the multi-wavelength photometric observations.

## 2 MODELS AND METHODS

We begin our presentation with discussion of models of companion stars, parameters of binary systems, and the supernova explosion model used in our study. These elements determine our choice of numerical methods and parameters of computer models, including hydrodynamic solvers and numerical discretization.

### 2.1 Stellar physics input

#### 2.1.1 Stellar companions and corresponding binary system models

Due to the unknown nature of supernova companions, it is important to consider various feasible binary systems in order to obtain a broad spectrum of outcomes to enable comparison with observations. In this work, we consider seven companion types: four MS stars, one SG star, and two RG stars. [Table 1](#) presents the properties of the companions and their respective binary systems. Our SG and RG model systems were obtained using the method of [Langer et al. \(2000\)](#), while our MS models were adopted from the existing model database (see [Table 2](#) in [Langer et al. \(2000\)](#)). For each model, we show the impact parameter,  $R_*/a$ , where  $R_*$  is the radius of the companion and  $a$  is the separation distance between the centers of the supernova and the companion. The impact parameter is similar for all systems considered, implying the orbital separation of  $a \approx 3R_*$ , similar to previous studies (see, e.g., [Marietta et al. 2000](#); [Pakmor et al. 2008](#); [Pan et al. 2012a](#)).

When selecting binary systems for our study, we aimed to cover a wide range of masses and orbital parameters for our progenitor systems. For example, the masses of our MS stars differ by about 50%, while their orbital separations (assuming the secondary fills its Roche lobe) differ by a factor of more than 3. The SG star has a mass equal to the most massive MS star, MS7, but is somewhat larger due to advanced evolution and consequently has a wider orbit. The two RG companions have significantly different radii and orbital separations. It is worth noting that despite the differences between the systems, the impact parameter differs only by about 30%.

#### 2.1.2 Supernova explosion model

We use a W7-like supernova model ([Nomoto et al. 1984](#)) to describe the structure of a exploding Chandrasekhar-mass, carbon-oxygen white dwarf. This model has been shown to closely match typical characteristics of observed SNIa events in terms of energetics and nucleosynthetic yields. Our model

has an explosion energy of  $\approx 1.15 \times 10^{51}$  erg, with the velocity of the ejecta linearly increasing with radius from its center to around  $30000 \text{ km s}^{-1}$  at its edge. The ejecta is chemically stratified with the core region dominated by the iron group elements, which is surrounded by a layer rich in intermediate mass elements. The outermost ejecta layers are composed of unburned carbon and oxygen.

### 2.2 Computational methods

It is interesting to note that despite continuous development of supernova-companion interaction models, the main conclusions of the original interaction model of [Marietta et al. \(2000\)](#) still stand. Taking into account three-dimensional effects (see, e.g., [Pakmor et al. 2008](#); [García-Senz et al. 2012](#)) or effects due to orbital motion and companion's spin ([Pan et al. 2012a](#); [Liu et al. 2012, 2013a](#)) proved to have only minor impact on the conclusions. Consequently, we decided to model the supernova-companion interactions in two spatial dimensions. Using this approach, we were able to study the evolution of the binary systems on large domains for relatively long times and at high resolutions. In what follows, we introduce our computational model including the hydro solver and mesh discretization, and describe the assumed initial and boundary conditions.

### 2.3 Hydrodynamics and relevant physics

In our study of ejecta-companion interactions, we use PROTEUS, a customized version of the FLASH 2.4 code ([Fryxell et al. 2000](#)) for the current application. FLASH is a finite volume multi-dimensional hydrodynamic block-structured AMR code. We solve the Euler equations using the PPM solver ([Colella & Woodward 1984](#)). In addition to solving transport equations for mass, momentum, and total energy, we also solve a set of equations describing advection of nuclear species and passive mass scalars. The chemical composition of our models is described using an extended alpha network with 19 isotopes; we do not include nuclear burning. The mass scalars are used to track the evolution of ejecta material, stellar material, and the ambient medium. We close the hydrodynamic system with the Helmholtz equation of state ([Timmes & Swesty 2000](#)). Finally, self-gravity is calculated using the multipole expansion of the Poisson equation with 10 moments.

In the study presented here, PROTEUS differed from the original FLASH code in regards to mesh refinement, treatment of passively advected mass tracers, and calculation of the gravitational potential. The latter modification was required due to the limited mesh resolution in our models, which required replacing the degenerate cores of RG companions with point masses. (The values of the point masses,  $m_{\text{pm}}$ , for RG319 and RG428 are given in [Table 1](#) in solar masses.) This procedure was not necessary in the case of SG or MS companions.

### 2.4 Computational domain and discretization

We simulate evolution of the binary systems in cylindrical geometry in two dimensions assuming axisymmetry. Thus, our computational domain starts at  $r = 0$  and extends to a

**Table 1.** Parameters of model binary systems and of their computational models.

Model designation	$m_*$ <sup>a</sup> [M <sub>⊙</sub> ]	$m_{\text{pm}}$ <sup>b</sup> [M <sub>⊙</sub> ]	$R_*$ <sup>c</sup> [R <sub>⊙</sub> ]	$a$ <sup>d</sup> [R <sub>⊙</sub> ]	$P$ <sup>e</sup> [d]	$R_*/a$ <sup>f</sup>	$r_{\text{max}}$ <sup>g</sup> [cm]	$t_i$ <sup>h</sup> [s]	$t_f$ <sup>i</sup> [s]
MS7	1.53	–	2.57	6.58	1.15	0.39	$5.86 \times 10^{13}$	$8.80 \times 10^1$	$2.00 \times 10^4$
MS38	1.15	–	1.07	2.94	0.37	0.37	$4.89 \times 10^{13}$	$4.00 \times 10^1$	$1.98 \times 10^6$
MS54	1.24	–	0.79	2.13	0.22	0.37	$3.61 \times 10^{13}$	$2.80 \times 10^1$	$2.00 \times 10^4$
MS63	1.13	–	1.40	3.84	0.55	0.36	$6.37 \times 10^{13}$	$5.30 \times 10^1$	$2.00 \times 10^4$
SG	1.53	–	3.18	8.15	1.59	0.39	$7.25 \times 10^{13}$	$1.10 \times 10^2$	$4.32 \times 10^4$
RG319	0.61	0.315	54.6	175	192	0.31	$2.49 \times 10^{15}$	$2.80 \times 10^3$	$8.64 \times 10^5$
RG428	0.75	0.423	249	755	1659	0.34	$1.14 \times 10^{16}$	$1.13 \times 10^4$	$5.78 \times 10^6$

<sup>a</sup> Mass of the binary companion.

<sup>b</sup> Mass of the point mass used to represent the degenerate core of the RG companion.

<sup>c</sup> Radius of the binary companion.

<sup>d</sup> Binary separation measured from the center of the supernova to the center of the companion.

<sup>e</sup> Orbital period of the progenitor system.

<sup>f</sup> Impact parameter.

<sup>g</sup> Radial extent of the domain.

<sup>h</sup> Initial simulated time.

<sup>i</sup> Final simulated time.

maximum radius  $r_{\text{max}} = d$ , with the domain extending from  $z_{\text{min}} = -d$  to  $z_{\text{max}} = +d$  in the z-direction. The characteristic size of the computational box,  $d$ , is about  $10^{13}$  cm for MS and SG models, and between  $10^{15}$  and  $10^{16}$  cm for the RG models (see Table 1 for detailed information of the sizes of the computational domains). We impose reflective boundary conditions along the symmetry axis, and allow for free outflow elsewhere. We assume isolated boundary conditions when calculating the gravitational potential.

We use an adaptive mesh discretization scheme wherein the mesh resolution is increased whenever the local variation of density exceeds 0.1 or pressure exceeds 0.2. The effective maximum mesh resolution of our simulations is defined as the number of cells per companion radius at the initial time. For every model family, we performed a series of simulations with resolution gradually increasing from 50 to 200 cells per companion radius. In what follows, we use a notation in which, for example, a model with 200 cells per companion radius is denoted as L200.

## 2.5 Initial conditions

We constructed the initial conditions in our simulations by mapping the supernova ejecta and the companion models onto the computational domain filled with an ambient gas of density of  $1 \times 10^{-16}$  g/cm<sup>−3</sup> and temperature of  $1 \times 10^4$  K. Mapping of the models to the mesh involved interpolation of density, temperature, and chemical composition. As we discussed earlier in Section 2.3, both the internal energy and the pressure were calculated using the Helmholtz equation of state.

The supernova was centered at the origin of our coordinate system with a radius scaled in such a way that it nearly filled its Roche lobe. We assumed that the supernova ejecta was isothermal with temperature of  $1 \times 10^8$  K. Also, as we discussed in Section 2.1.2, we assumed that the ejecta was homogeneously expanding. The supernova explosion energy was roughly equal to  $1.15 \times 10^{51}$  erg. Additionally, we adjusted initial simulation times to account for the geometrical expansion of the supernova model. In this way, simulation

times for various models can be directly compared with  $t = 0$  corresponding to the supernova explosion time.

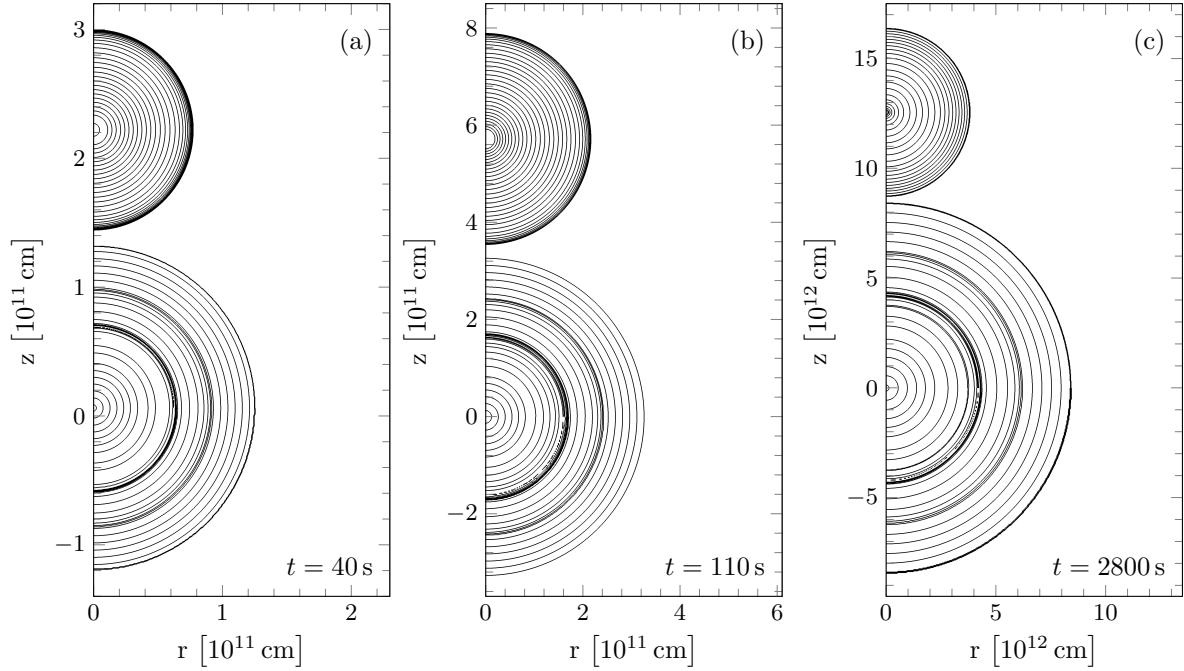
The stellar companion was placed in the positive direction along the symmetry axis at the distance from the origin defined by the orbital distance of the binary system model (cf. Table 1). Before being interpolated onto the mesh, the original companion model was iteratively relaxed to hydrostatic equilibrium. This procedure was necessary in order to eliminate unbalanced pressure gradients due to the differences between the equation of state used to obtain the original companion model and the Helmholtz equation of state. The relaxed companion structure, along with the supernova ejecta model, was then mapped down to the mesh.

Fig. 1 shows the density distribution at the initial time for the MS38, SG, and RG319 binary systems. The density is shown with 30 contours logarithmically spaced between the density values specifically chosen for every system. The dynamic range of the density plot shown changes between 6 orders of magnitude for the MS38 (Fig. 1(a)) and SG (Fig. 1(b)) models, and 7 orders of magnitude for the RG319 model (Fig. 1(c)). Due to the aforementioned pre-expansion of the supernova ejecta, the initial times differ from 40 seconds for the MS38 model to almost 1 h for the RG319 model.

The binary interaction models were evolved as long as the supernova shock was fully contained inside the domain. Thanks to this constraint, we can fully account for different materials (as tracked by corresponding mass scalars) in our analysis. Also, the interior pressure of the expanding ejecta is unaffected by rarefaction waves that may be produced as a result of the shock crossing the domain boundaries. The final times for each model are shown in Table 1.

## 3 RESULTS

We present the results of our simulations using a representative subset of our binary models for the MS companion system MS38; subgiant system, SG; and red giant system, RG319. The evolution in the remaining cases of MS and RG



**Figure 1.** Density contour maps of a selected subset of model binary systems at their initial simulation times. The density is shown with 30 logarithmically spaced contour lines for (a) the main-sequence companion MS38 ( $10^{-4} - 10^2 \text{ g cm}^{-3}$ ), (b) the subgiant SG ( $10^{-5} - 10^1 \text{ g cm}^{-3}$ ), and (c) the red giant RG319 ( $10^{-10} - 10^{-3} \text{ g cm}^{-3}$ ). Note that the initial simulation times and domain sizes differ between the panels.

companions does not qualitatively differ from those included in the subset. The models presented in this section were obtained at the resolution of L200.

In our presentation, we focus on the general development of the flow, the propagation of the supernova shock through the companion interior and the surrounding circumstellar medium, and the process of mixing between the ejecta and companion’s envelope. In each case presented here, the overall evolution and flow morphology bears close resemblance to that of a supersonic flow past a sphere [Hayes & Probstein \(2004\)](#). In that case, a bow shock forms at some distance from the object, and the object becomes engulfed in a shocked gas. Provided the fluid viscosity is sufficiently low, as is the case in the situation considered here, a boundary layer forms close to the surface of the object. This boundary layer eventually separates from the body, and the flow recirculates and converges further downstream from the object forming a turbulent wake [van Dyke \(1982\)](#).

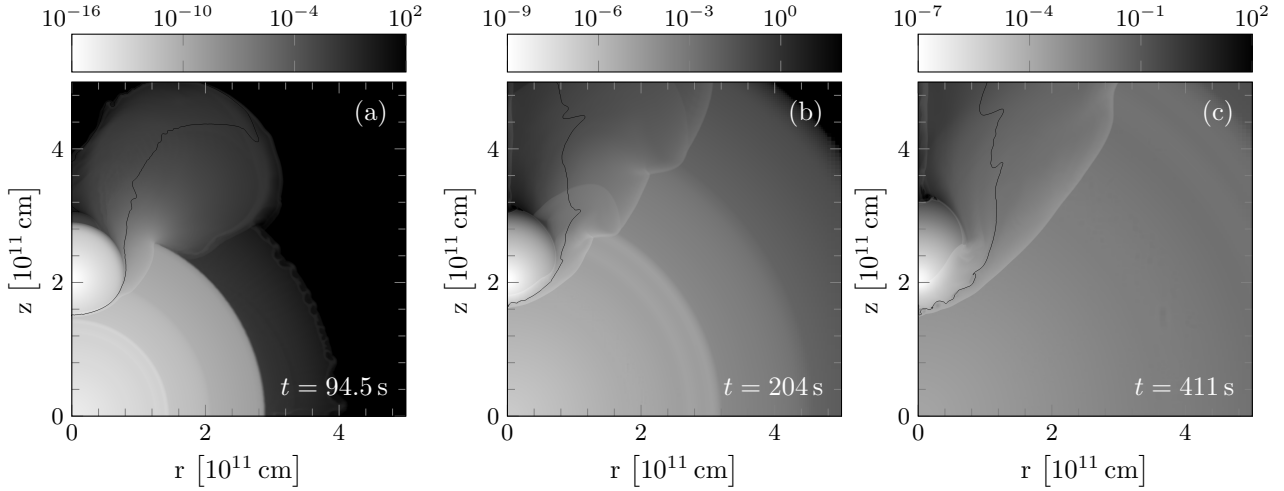
### 3.1 Binary system with main sequence companion MS38

Fig. 2 shows details of the interaction between the supernova ejecta and the MS companion in the MS38 model. Fig. 2(a) shows the density structure about a minute after the simulation has started. At this time, a pair of shocks exist within the supernova-companion interaction region. The first shock is the original supernova shock transmitted into the stellar companion, which by this time has penetrated around one third of the stellar radius toward the companion’s center. The second shock is the reflected shock, which formed when the original supernova shock hit the steep density gradient of

the outer layers of the stellar companion. This shock moves into the supernova ejecta. The two post-shock regions are separated by a contact discontinuity, which delineates the shocked supernova ejecta from the shocked companion material. The contact discontinuity is depicted in Fig. 2(a) with a solid line starting at  $(r, z) \approx (0, 1.5 \times 10^{11}) \text{ cm}$ . The contact line is visibly flattened near  $r = 0 \text{ cm}$ , indicating the compression of the companion’s envelope due to interaction with the supernova ejecta.

The structure is somewhat more complex in the region behind the companion. At the time of Fig. 2(a), the companion is already completely engulfed in the shocked material. The material stripped from the companion begins to accumulate in the region behind ( $z > 2.9 \times 10^{11} \text{ cm}$ ) the companion, which is customarily identified as the “ejecta hole.” Further away from the symmetry axis, the stripped material is separated from the ejecta by the contact discontinuity (the solid line passing near  $(r, z) = (1.2 \times 10^{11}, 4 \times 10^{11}) \text{ cm}$ ). The contact discontinuity is located inside a large, bubble-like region created when the high pressure, doubly-shocked material (overrun first by the main supernova shock and then by the reflected shock) provided additional pressure support for the main supernova shock. Thus, this region is bounded from the outside by the supernova shock.

The shock transmitted into the companion’s interior weakens around the progenitor’s perimeter as the contribution of the ram pressure of the supernova shock decreases. Similarly, the reflected shock becomes gradually weaker, although it remains strong enough to move laterally into the rapidly expanding, low-density ejecta (visible as a density jump located near  $(r, z) = (2.3 \times 10^{11}, 2.6 \times 10^{11}) \text{ cm}$ ). The lower part of the expanding supernova remains unaffected by the supernova-companion interaction. The outer edge of the



**Figure 2.** Pseudocolor maps of density distribution in the MS38 model. (a)  $t = 94$  s; (b)  $t = 203$  s; (c)  $t = 411$  s. In each panel, a contour line denotes the position of the contact discontinuity separating the ejecta from the stellar companion material. Note that the density scale changes between the panels. See text for details.

expanding structure is composed of a layer bounded by the supernova shock on the outside and by a reverse supernova shock on the inside. The contact discontinuity separating the shocked ambient medium material from the shocked ejecta displays a complicated structure due to Rayleigh-Taylor instability (RTI).

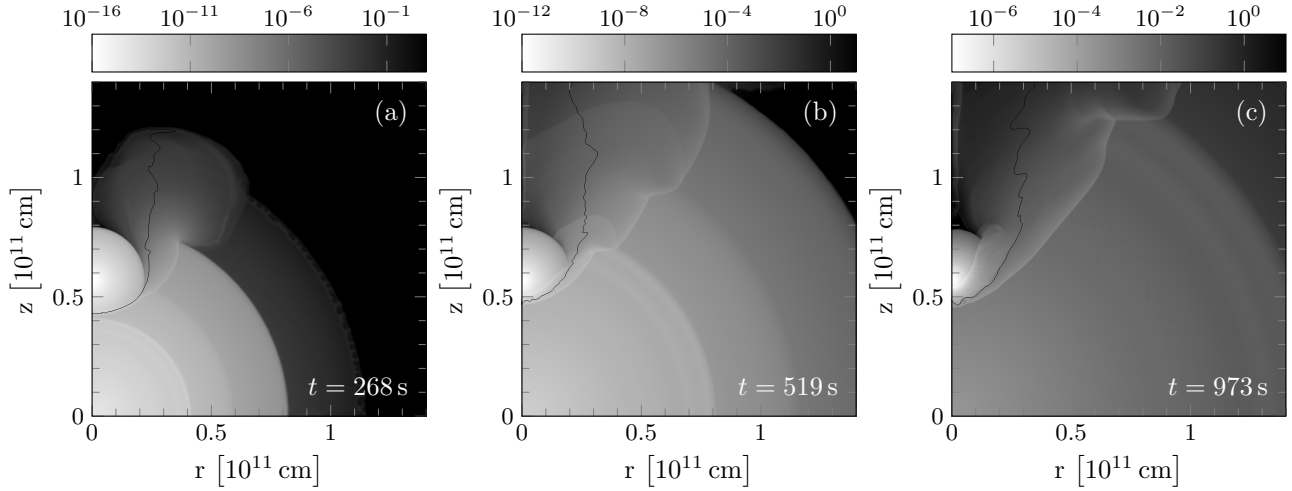
As the time progresses, the transmitted shock continues to move through the stellar companion, and by  $t = 204$  s it penetrates to about two-thirds of stellar radius towards the center (see Fig. 2(b)). The contact surface separating the shocked stellar envelope from the shocked supernova ejecta begins to show the first signs of Kelvin-Helmholtz instability (KHI) near  $(r, z) = (0, 1.7 \times 10^{11})$  cm. This is due to progressively increasing shear as the shocked ejecta flows around the companion star. The region bounded by the transmitted and reflected shock now contains a significant amount of material heated to temperatures around  $5 \times 10^7$  K, which has been predicted to produce a significant amount of X-ray emission (Kasen 2010). We should point out that much higher temperatures ( $9 \times 10^9$  K) are observed in the post-shock region of the supernova shock. However, it is not expected that this material is going to produce any significant amount of emission as the amount of mass involved is small. At the time shown in Fig. 2(b), the reflected shock continues to move into the ejecta and its front is composed of three distinct segments. This rather unusual shape of the shock front is due to the density stratification of the ejecta. Another new flow feature visible at this time is a conical shock located near the center of the low-density region behind the companion. This shock is relatively weak compared to other shocks present in this problem, and it would likely be weaker in simulations that do not assume symmetry.

Fig. 2(c) shows the structure of the interaction region at  $t = 411$  s. By this time the transmitted shock has reached the stellar companion's core. The Kelvin-Helmholtz instability at the interface separating the supernova ejecta from the stellar material is now well developed, while the temperatures decreased slightly to  $2 - 3 \times 10^7$  K. The companion's layers and the ejecta shocked and compressed at the begin-

ning of the interaction process, which includes the region associated with KHI, have now begun to expand with velocities of up to  $500 \text{ km s}^{-1}$ . Additionally, further along the interface, as the shear increases and the compression decreases, the outer layers of the companion are mixed with the ejecta and carried away downstream with the flow. The stripped material is advected around and past the companion, continuing to fill the low-density region behind the companion.

### 3.2 Binary system with subgiant companion SG

The evolution in the case of the SG companion proceeds qualitatively in a very similar manner as the main-sequence companion discussed in Section 3.1. The noticeable difference at early times ( $t = 268$  s, Fig. 3(a)) is that the hemisphere of the companion facing the ejecta is visibly more compressed due to the more extended envelope of the SG. The incoming ejecta is thus able to impart greater pressure upon the more flat surface of the companion. (The geometrical effects, such as the differing orbital distance, do not play a part here. This is because in our models the secondary fills its Roche lobe and the companion occupies nearly the same solid angle as seen from the explosion center.) The transmitted shock is thus able to compress relatively larger portion of the envelope. This increase in the efficiency of the interaction can be seen by comparing the location of a kink at the surface of the transmitted shock (visible near  $(r, z) = (0.7 \times 10^{11}, 2.2 \times 10^{11})$  cm and  $(r, z) = (0.2 \times 10^{11}, 0.62 \times 10^{11})$  in Fig. 2(b) and Fig. 3(b), respectively.) The kink is associated with a point where the ejecta is no longer able to drive a strong shock into the envelope. The more efficient energy transfer from the ejecta into the envelope also enhances the process of stripping of the envelope material from the companion, when compared to the more compact main-sequence companion. At the time when the transmitted shock has reached the companion's center ( $t = 973$  s in Fig. 3(c)), and in contrast to the main-sequence model (cf. 2(c)), almost the entire envelope has been overrun by the transmitted shock. Furthermore, KHI



**Figure 3.** Pseudocolor maps of density distribution in the SG model. (a)  $t = 268$  s; (b)  $t = 519$  s; (c)  $t = 973$  s. In each panel, a contour line denotes the position of the contact discontinuity separating the ejecta from the stellar companion material. Note that the density scale changes between the panels. See text for details.

is visibly less active along the contact discontinuity separating the shocked envelope and the shocked ejecta. This is because the density contrast across the contact discontinuity is lower than in the case of the more compact main-sequence companion (and the velocity shear is weaker).

### 3.3 Binary system with red giant companion RG319

Apart from the difference in temporal and spatial scales, the evolution in the case of the RG319 binary proceeds in a similar fashion to that in the SG system described in Section 3.2. For example, the compression of the companion’s envelope at early times (Fig. 4(a)) is only marginally stronger than the compression seen in the SG case. Also, similar to the SG case, the KHI does not grow because of the lower density contrast across the contact discontinuity and the weaker shear (Fig. 4(b)). Finally, because the envelope has a much lower density than in the SG case, the variations in the ram pressure provided by the ejecta are now more easily communicated to the reflected shock. Eventually this leads to the “segmentation” of the reflected shock front (Fig. 4(c)).

## 4 DISCUSSION

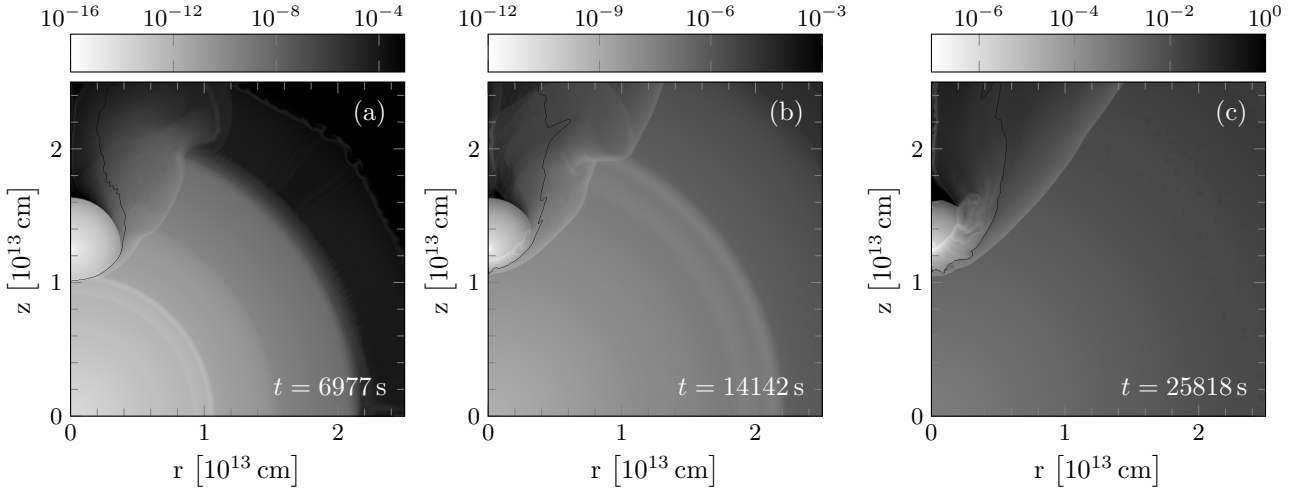
### 4.1 Structure of the ejecta hole

Fig. 5 shows the structure of our supernova-companion interaction models at the final simulated times. The ejecta hole is visible in each figure panel in the upper half of the computational domain, extending from the symmetry axis. The surface of the conical region is bounded by the reflected (bow) shock, which appears “segmented” due to stratification of the ejecta (cf. Section 3.1). The innermost regions of the hole are filled with the material stripped from the companion, and the solid line marks the contact discontinuity separating the companion’s material from the supernova ejecta. The abundance of the companion’s material in the hole gradually decreases with radius from the companion

toward the supernova shock front, and is completely mixed with the ejecta at the shock front. Although much of the companion’s material is confined near the center line of the hole, small amounts of companion material can be found throughout the hole region. Trace amounts ( $\sim 1 \times 10^{-4}$ ) of the companion’s material can also be found further away from the hole’s center line along the surface of the supernova. This contamination occurred during the early stages of the interaction and affects a region extending 15-30 degrees outside the bow shock.

The geometry of the hole has been discussed in detail by a number of authors. [Marietta et al. \(2000\)](#) originally reported the ejecta hole to have an opening angle between 30 and 40 degrees depending on the ejecta velocity (supernova explosion energy), with narrower holes produced by ejecta with higher velocities. These results appeared independent of the companion type (MS star, SG, and RG) [Pakmor et al. \(2008\)](#) found the holes with opening angles about 45 degrees for their series of main-sequence companions. Later on, [García-Senz et al. \(2012\)](#) reported holes with opening angles of 40 degrees for their single MS model considered (independent of the model dimensionality or whether the orbital rotation was accounted for or not). Around the same time, [Pan et al. \(2012a\)](#) reported results of more than twenty models of binaries containing MS, helium, and RG companions. In their study, the hole opening angle varied between 30 degrees for the compact helium companion to up to 50 degrees for their RG companion model star.

Our results are largely consistent with the previous findings. To illustrate the overall density distribution in the models, we calculated an equivalent surface mass,  $m_D$ . This quantity has been obtained along radial rays originating at the symmetry axis at the height corresponding to location of the maximum model density (the central density of the companion). Starting from the origin of the so-defined coordinate system, we divided rays in a number of small radial segments. The beginning and the end of each segment were then used to define the inner and outer radius, respectively, of spherical shells. The mass of each shell was obtained by mul-



**Figure 4.** Pseudocolor maps of density distribution in the RG319 model. (a)  $t = 6977$  s; (b)  $t = 14142$  s; (c)  $t = 25818$  s. In each panel, a contour line denotes the position of the contact discontinuity separating the ejecta from the stellar companion material. Note that the density scale changes between the panels. See text for details.

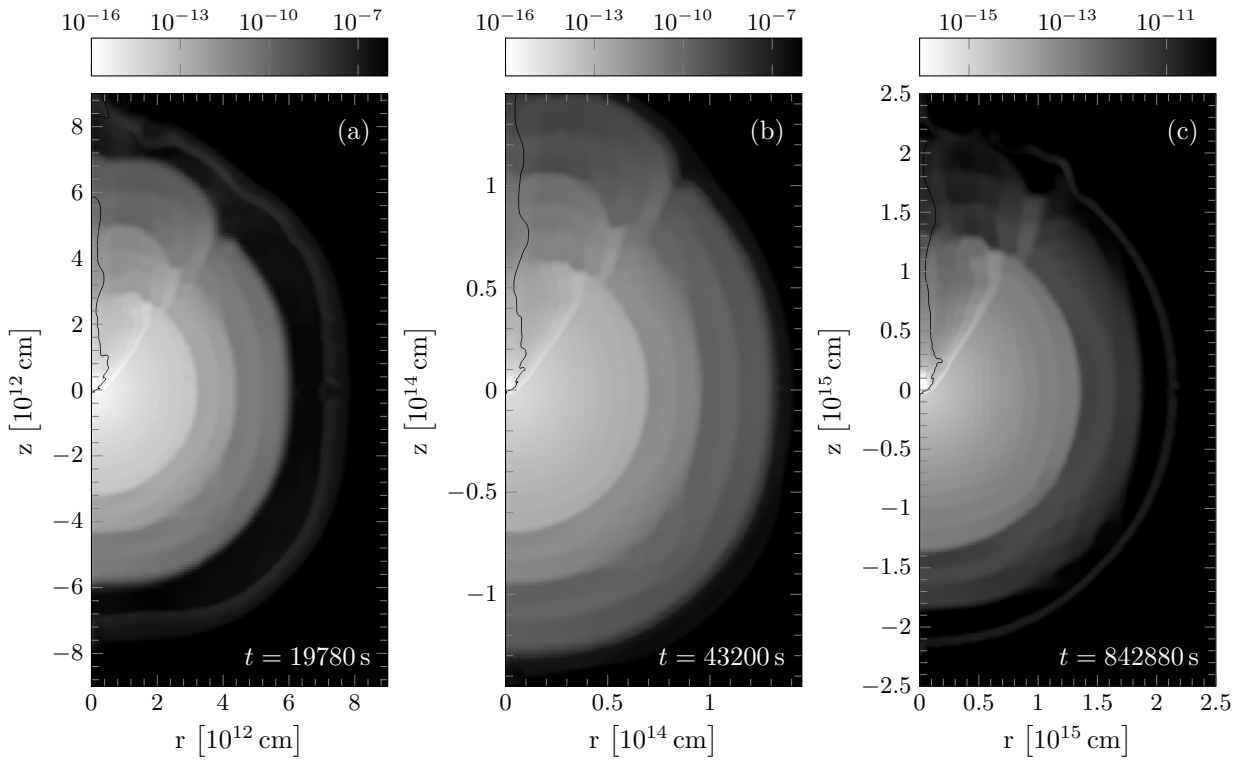


**Figure 5.** Pseudocolor maps of density distribution in a subset of our binary system models at the final simulated times. (a) MS38 ( $t = 19780$  s); (b) SG ( $t = 43200$  s); (c) RG319 ( $t = 842880$  s). In each panel, a contour line denotes the position of the contact discontinuity separating the ejecta from the stellar companion material. Note that the density scale and spatial scale changes between the panels. See text for details.

tipling its volume by the density interpolated at the point located at its average radius. In the last step, the equivalent surface mass was obtained by summing up mass contributions from all the shells except for the material bounded to the companion. In other words,  $m_D$  measures the total mass of a spherically symmetric configuration whose radial density profile is identical with the density profile measured at

a given time along rays originating from the approximate companion center. The left panel in Fig. 6 shows the dependence of the equivalent surface mass as a function of the polar angle for both the (unbound) companion material and the supernova ejecta. In the majority of the models, with the exception of the red giant RG319 binary system, the density reaches the maximum between 40 and 50 degrees away



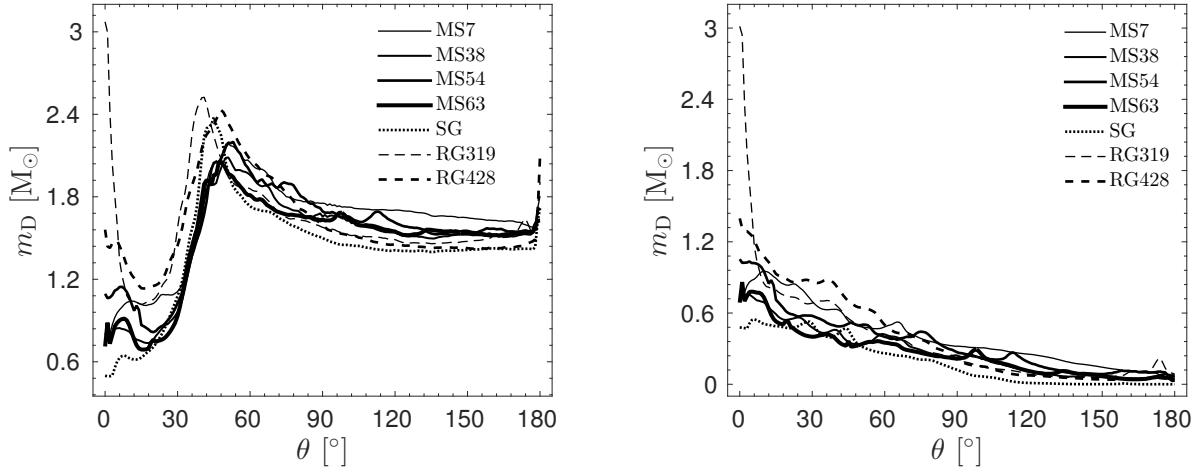


**Figure 6.** Angular distribution of the equivalent surface mass,  $m_D$ , at the final simulated times. The mass is accumulated along radial rays originating from the center of the companion star. The angle of  $0^\circ$  corresponds to the ray aligned with the symmetry axis pointing in  $z > 0$  direction. (left panel) The unbound stellar material and the supernova ejecta material. (right panel) The unbound stellar material only. The mass distributions are shown with solid, dotted, and dashed lines for the MS, SG, and RG binary systems, respectively; see text for details.

from the symmetry axis. This angle defines the half-opening angle of the ejecta and the location of the edge of the hole. The density gradually decreases from the edge into the region outside the hole. The inner part of the hole’s edge is relatively well-defined with the density rapidly decreasing, while the density begins to increase inside the innermost 10–15 degrees. This increase in density near the center line of the hole is due to accumulation of mass stripped from the companion. This is clearly visible by comparing the distribution of the equivalent surface mass for both the unbound stellar material and the supernova ejecta (left panel in left panel in Fig. 6) to that of the unbound stellar material only (right panel in Fig. 6).

We found the greatest accumulation of stripped material in RG models that have the most extended, weakly bound envelopes, while we observed the least accumulation in the case of the compact SG. The amount of stripped mass appears approximately linearly decreasing from the symmetry axis up to at least  $120^\circ$  away from the center line of the hole. No stripped material is observed at greater angular distances from the hole in the case of the SG model, where in other models the amount of stripped material observed in those regions does not exceed 10 per cent of the typical values found near the hole’s center.

#### 4.2 Amount of stripped mass

To estimate the amount of mass lost by a stellar companion, we compared its initial mass (cf. Table 1) to the amount of gravitationally bound stellar material found at the final simulation time. Table 2 shows the final masses of and relative mass lost by our companion model stars. For the given supernova explosion (energy, ejecta mass) and orbital (distance, Roche-filling factor) parameters, the gravitational binding energy of the companion star is the key factor that determines how much mass the companion will lose during the interaction with the supernova.

**Table 2.** Total amount of mass stripped from the companion,  $\Delta m$ , and the fraction of each companion’s initial mass that was stripped,  $\Delta m/m_*$ , at the final simulated times.

Model designation	$\Delta m$ [ $M_\odot$ ]	$\Delta m/m_*$
MS7	0.37	0.24
MS38	0.25	0.22
MS54	0.32	0.26
MS63	0.24	0.21
SG	0.17	0.11
RG319	0.28	0.41
RG428	0.33	0.44

The mass stripping process was the most efficient in the case of RG model binaries, in which case both red giant companions lost their entire envelopes. The typical amount of mass stripped in the case of MS companions was slightly over 20 per cent, while only about 10 per cent of the companion mass was lost in the case of the SG. The observed amounts of stripped mass are not surprising given that the envelope stripping process sensitively depends on the binding energy of the envelope. In addition, the mass loss occurs primarily during the first hour of the interaction in the case of SG and MS companions, and between half a day and one day in the case of RG companions.

The relative amount of stripped mass in the case of our MS binary models varies between 21 and 26 per cent. This is typically higher than the amounts of stripped mass reported by Marietta et al. (2000) ( $\approx 15$  per cent for their HCV model), Pan et al. (2012a) ( $\approx 16$  per cent in their 2D, non-rotating, Roche-lobe-filling MS-2D-Nr model), and Liu et al. (2012) (between 6 and 24 per cent across their MS models). The mass loss found in our MS models approximately follows the power-law relation between stripped mass and orbital separation obtained by Pakmor et al. (2008). However, the obtained mass loss is 30–60 per cent greater than estimate given by equation 4 in Pakmor et al. (2008), even once

corrected for the differences in supernova explosion energies (using equation 2 in Pakmor et al. (2008)). Our results are marginally consistent with the results presented by García-Senz et al. (2012), who reported a mass loss of around 10 per cent.

In the case of a SG companion, Marietta et al. (2000) reported a mass loss on the order of 15 per cent for their HCVL model, which favorably compares to the estimated mass loss found in our SG model. These estimated amounts of mass lost by SG companions exceed by a factor of about 3 the mass loss reported by Pan et al. (2012a) for their compact helium companion model. Finally, the groups who studied the interaction between the supernova and the RG companions (Marietta et al. 2000; Pan et al. 2012a) uniformly found the companion stars completely stripped of their envelopes, as is the case in our study.

We note that the results of Pakmor et al. (2008), who reported a mass loss of up to 5 per cent in their set of MS models, remains an outlier in this series of studies of binaries with MS companions. The difference in mass loss predicted in that study appears most likely as a result of their use of companion models that were not computed self-consistently in binary system evolution. (The later followup study by Liu et al. (2012) who used companion models computed with a binary stellar evolution code produced mass loss estimates similar to those obtained by other groups.)

### 4.3 Kinematic properties of stripped companion material

Because no substantial amounts of hydrogen or helium are expected to exist in the supernova ejecta, detection of hydrogen or helium lines in the Type Ia supernova spectra would provide strong evidence for the presence of a non-degenerate companion in the system. Therefore, such detection would not only confirm the single-degenerate scenario for SNIa formation, but also allow to distinguish between the supernovae originating in different channels. Marietta et al. (2000) were the first to provide estimates of the amount and velocity distribution of hydrogen and helium stripped from the non-degenerate companion stars. Their results indicated that the typical velocity of the stripped hydrogen, defined as the half-mass point of the mass distribution in velocity space, was about  $800 \text{ km s}^{-1}$  for their compact MS companion model, nearly  $900 \text{ km s}^{-1}$  in the case of their SG companion, and between  $400$  and  $600 \text{ km s}^{-1}$  for their RG companions.

Fig. 7 (left-hand panel) shows the mass distribution in velocity space in our MS38 binary model. The velocity distribution of the ejecta material matches that reported by Marietta et al. (2000) closely, as expected due to the use of the same explosion model. The difference in the average velocities,  $v_{1/2m}$ , can in part be explained by the supernova explosion energy employed by Marietta et al. (2000) being approximately 7 per cent higher than in our model. The other contributing factor, as we discuss below in the context of the Pan et al. (2012a) work, might be lower mesh resolution used in the Marietta et al. (2000) study.

The overall shape of the total stripped mass distribution, and also hydrogen and helium distributions, found in our MS38 model is also similar to those reported by Marietta et al. (2000). We find higher amounts of stripped material for a given velocity, which reflects the fact that we find

more stripped material in all of our models. Additionally, as we mentioned earlier, the higher supernova explosion energy used in Marietta et al. (2000) could be responsible for their higher average velocities of the stripped material,  $v_{1/2m}$  ( $823 \text{ km s}^{-1}$  in their HCV model compared to our MS38 result of approximately  $657 \text{ km s}^{-1}$ ). The only major qualitative difference is the presence of a distinct low-velocity cutoff in the stripped mass in our simulations. After careful examination of the data, we found that the velocity associated with the cutoff in our results corresponds to the velocity of the material that has zero binding energy. This implies that at this particular moment during the evolution, the material with near-zero binding energy is not in hydrostatic equilibrium, and instead continues to expand away from the secondary. At later times, however, it will fall back to the star. Because the velocity distributions shown in Marietta et al. (2000) do not display such a low-velocity cutoff, and evolutionary times in their corresponding simulations are identical to ours, we conclude that the dynamics of the material with near-zero binding energies differ.

Much of the same conclusions can be drawn from comparing the velocity distribution of stripped material in our SG model (shown in the center panel in Fig. 7) to that of the HCVL model of Marietta et al. (2000). The average velocity distribution in our SG model is approximately  $642 \text{ km s}^{-1}$ , lower than the value reported in their work ( $890 \text{ km s}^{-1}$ ). Also, our velocity distributions indicate greater amounts of stripped material than those reported by Marietta et al. (2000) (cf. Table 2). Finally, in the case of our RG319 model, the average velocity of the stripped companion's material (approximately  $562 \text{ km s}^{-1}$ ) compares favorably to that reported by Marietta et al. (2000) in the case of their HALGOLa model ( $593 \text{ km s}^{-1}$ ). However, the amount of mass stripped in our model (approximately  $0.3 M_{\odot}$ ) is less than the amount reported in their study ( $0.54 M_{\odot}$ ).

Liu et al. (2012) presented analysis of velocity distributions of stripped material only for one of their main-sequence models. Based on fig. 10 in their paper, we estimated the half-mass velocity of the stripped material to be around  $1400 \text{ km s}^{-1}$ . This is remarkably higher than the average velocity reported by Marietta et al. (2000), although both groups used identical supernova explosion energies. It is also substantially higher than indicated by the simulations of Pakmor et al. (2008) (as reported by Liu et al. (2012)). One possibility for this discrepancy could be a difference in the companion models. However, our analysis of a similar in mass MS companion, MS54, showed a half-mass velocity of about  $600 \text{ km s}^{-1}$ . The results presented by García-Senz et al. (2012) do not allow for a quantitative comparison, however the overall shape of the velocity distribution is similar to that found in our MS38 main sequence model. Also, our velocity distributions are higher by a factor of about 5 than those reported in their work. However, it seems difficult to reconcile that difference solely with their supernova model explosion energy being only 20 per cent lower than that of our model supernova.

We observe much better qualitative agreement of velocity distributions of stripped material between our results and those reported by Pan et al. (2012a). Although we cannot compare the actual values of the velocity distributions due to differing units used to present the results, the distributions presented by Pan et al. (2012a) show distinct low-velocity

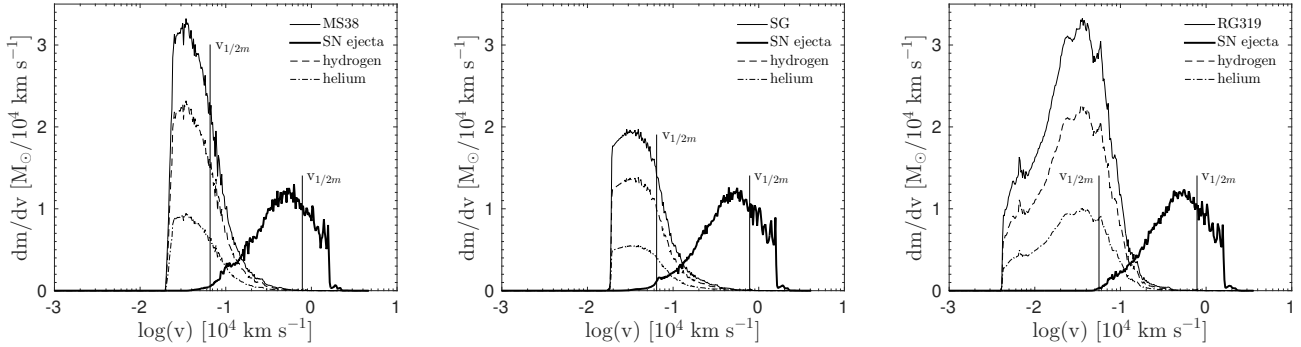


**Figure 7.** Velocity distribution of the unbound companion material and the supernova ejecta for a subset of companion models at the final simulated times. (left panel) the main-sequence companion MS38; (middle panel) the subgiant SG; (right panel) the red giant RG319. For each model, the mass distribution is shown for hydrogen (dashed line), helium (dash-dotted line), the total stripped companion material (thin solid line), and the supernova ejecta (thick solid line). Short vertical lines indicate the average velocities of the stripped companion material (left vertical line) and the supernova ejecta (right vertical line). Note that the velocity is shown in log scale. See text for discussion.

cutoffs in the case of their MS and helium companions while the velocity distribution extends to low velocities in the case of their RG model system. The velocities corresponding to the maximum mass distributions (not to be confused with the average velocity,  $v_{1/2m}$ , discussed above) reported by Pan et al. (2012a) were, however, substantially higher than those found in our models. More specifically, the peak velocities of the stripped material were by about 30 per cent, 60 per cent, and 40 per cent lower in the case of our MS, SG, and red giant models, respectively. It is unlikely that the lower supernova explosion energy used in our study is responsible for these substantial differences in peak velocities of stripped material. This is because the explosion energies used in the two studies differs by only a few per cent. We conclude that either the significantly lower mesh resolution or the particle-based analysis method used by Pan et al. (2012a) are likely factors responsible for the observed differences in the energetics of the stripped material.

#### 4.4 Stripped hydrogen-rich material at high velocities

We conclude our discussion of kinematic properties of stripped material by focusing on hydrogen within its high velocity tail. As originally pointed out by Marietta et al. (2000), the distribution of hydrogen at high velocities is potentially an important observationally accessible diagnostic allowing to discriminate between various types of companion stars. Fig. 8 shows the accumulated amount of stripped hydrogen mass with velocities greater than the given velocity for our set of binary system models. Several important characteristics of the hydrogen mass velocity distributions can be noted. Despite the diversity of our main sequence model sample, their hydrogen mass velocity distributions are very similar. In addition, the distributions for all companion models are similar for velocities below approximately  $13\,000\text{ km s}^{-1}$ . At higher velocities, companions of different types fold into distinct groups. For example, we can clearly distinguish between the SG model and MS models, with the SG containing a greater amount of mass at a given velocity. Both RG models, especially the most extended RG428

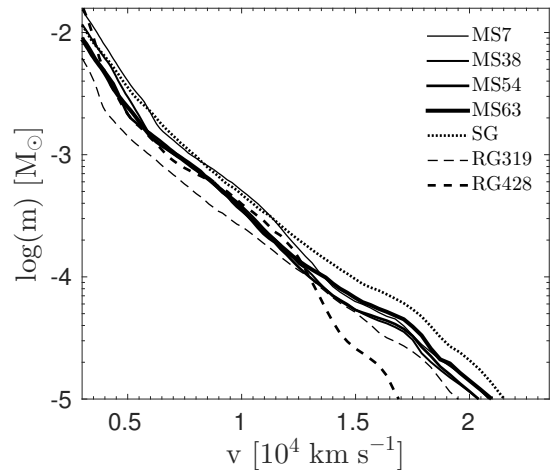


**Figure 8.** The amount of mass with velocities higher than a given value for unbound companion material at the final simulated times. The accumulated mass distributions are shown for MS, SG, and RG companions with solid, dotted, and dashed lines, respectively. Note that the accumulated mass is shown in log scale; see text for details.

companion, produce the least amount of high velocity hydrogen, and should be relatively easily distinguishable from other companion types. The amount of hydrogen mass moving with the velocities above  $15\,000\text{ km s}^{-1}$  in the SG model is by a factor almost 4 greater than that of the RG428 model.

Our accumulated hydrogen masses as a function of velocity can be compared to the results of Marietta et al. (2000) (see their fig. 32). Although the overall run of the distributions appears very similar between the two studies, the hydrogen mass distributions are not as clearly separated in the Marietta et al. (2000) study than in our models. There is potential confusion between various companion models in their study at velocities around  $19\,000\text{ km s}^{-1}$ , and the distributions cross over again at around  $13\,000\text{ km s}^{-1}$ . The amount of hydrogen mass moving faster than  $15\,000\text{ km s}^{-1}$  in the Marietta et al. (2000) study differs by a factor of about

2.6 between their models, which is somewhat less than the factor of almost 4 found in the present work. It is conceivable that the differences in the kinematics of the stripped hydrogen found in our simulations as compared to those of Marietta et al. (2000) can be due to a number of differences between the models such as model resolution, structure of companion stars, and supernova explosion energy. Although we cannot clearly identify the source of the differences, the observed variations in the stripped hydrogen kinematics provide initial insight into the uncertainties of the model predictions based on this kind of diagnostic.

#### 4.5 Chemical contamination of companion

It is conceivable that the supernova ejecta could deposit its material onto the companion. Thus, the presence of lines of elements that are not produced in low mass stars would provide evidence for the interaction between the companion and the supernova. To quantify the level of contamination of the companion by the ejecta, we calculated the amount of  $^{56}\text{Ni}$  that was bound to the companion star at the final simulated time. The amounts of companion-bound nickel were less than  $10^{-8} M_{\odot}$  in the case of the MS companions, around  $10^{-7} M_{\odot}$  in the case of the SG, with only trace amounts of  $^{56}\text{Ni}$  found in the case of RG companions.

The estimated levels of contamination are relatively small compared to other studies. Marietta et al. (2000) found that approximately  $1.3 \times 10^{-4} M_{\odot}$  of iron-rich supernova material was bound to the companion star in their MS model at the end of their simulation. Their estimate was by a factor of about 10 higher than the approximately  $10^{-5} M_{\odot}$  reported by Pan et al. (2012a) in the case of their three-dimensional model of supernova interaction with the MS companion. Additionally, the work by Pan et al. (2012a) is the only study that considered contamination of post-MS companions. In particular, they reported a relatively low, but still significantly higher than found in our model, contamination of their RG binary companion by  $10^{-8} M_{\odot}$  of  $^{56}\text{Ni}$ . We are not in a position to compare contamination estimation in the case of our SG model to the helium model of Pan et al. (2010) or Pan et al. (2012a), as the two binary systems and companions differ substantially.

Because the amounts of ejecta material contaminating the secondary stars found in this work and in the previous studies are relatively small, it is conceivable that these estimates are subject to numerical effects and certain model assumptions. In particular, we note that in our MS models and in the case of our SG model, the ejecta material bound to the secondary is the least mixed in the region close to the symmetry axis and on the hemisphere of the secondary that faces the explosion site.

The degree of mixing of the ejecta material with the envelope material of the companion gradually increases further away from the symmetry axis. This is chiefly because the primary mechanism for mixing in the interaction models is shear between the supernova ejecta and the stellar material. The shear is the least near the symmetry axis, which explains the relative purity of ejecta material bound to the companion. The outcome would almost certainly be different in more realistic models that would account for the orbital motion and the spin of the companion, as considered by Pan et al. (2012a). In particular, these authors

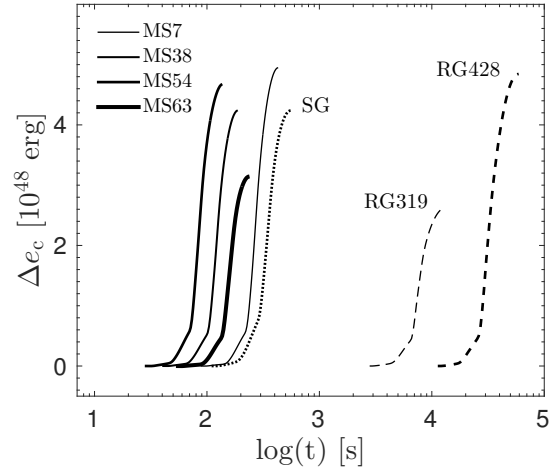


**Figure 9.** Change in internal energy of companion material in respect to the initial internal energy as a function of time. The energy change is shown with solid, dotted, and dashed lines for MS, SG, and RG models, respectively. The curves terminate at the times when the maximum energy change was recorded. Note that the time is shown in log scale; see text for details.

found a substantial degree of mixing of the ejecta and stellar companion material in the case of their helium model (cf. left panel of fig. 23 in (Pan et al. 2012a)). Because the amounts of ejecta material contaminating the companion are subject to strong numerical effects, as discussed in Section 4.7, predictions based on low-resolution models should be considered preliminary. In addition, as originally noted by Marietta et al. (2000), the truthful estimates of contamination levels of companions would require simulations covering much longer evolutionary times to allow for accretion of ejecta material originally located close to the ejecta center and, therefore, moving at relatively low speeds.

#### 4.6 Properties of transient X-ray source

The supernova shock interaction with the companion serves not only to heat the companion’s outer layers, but also the ejecta itself due to the formation and propagation of the reflected shock, as we described in Section 3.1. A semi-analytic model shown by Kasen (2010) predicts that the ejecta heated by the reflected shock may produce a highly luminous burst ( $L \approx 10^{44} \text{ erg s}^{-1}$ ) of soft X-rays. This theoretically predicted emission would dominate the supernova luminosity for up to a few days, depending on the companion type, and be strongly angle-dependent with most radiation emitted through the (least opaque) hole region carved out in the ejecta by the companion. Due to the hole geometry, the external observer may have a chance to see the resulting soft X-ray/UV flash of radiation in about 10 per cent of Type Ia events (originating from a single degenerate formation channel).

The shock-heating process of the stellar envelope in all of our model binary systems is illustrated in Fig. 9. The evolution of the internal energy change (compared to the initial internal energy) in every model is shown with a curve starting at the initial simulation time and terminating at the time when the maximum change of internal energy due to

heating is recorded,  $t = t_h$ . We do not show the data past that point in time, as the evolution of the internal energy of the companion becomes affected by its expansion and mixing of the envelope material with the ejecta. The time over which the companion is heated chiefly depends on the companion's size. It varies from as little as 80 seconds in the case of the MS54 companion to as much as nearly half a day in the case of the RG428 model giant. The estimated amount of energy stored during that time, along with the energy stored in the ejecta, as discussed below, provides the energy budget for the prompt radiation burst.

The contribution of the heated envelope component to the radiation flash was not considered by Kasen (2010), who focused on the evolution and emission of the ejecta.<sup>1</sup> Furthermore, the shocked ejecta and the shocked envelope material are subject to mixing due to Kelvin-Helmholtz instability (cf. Section 3). This mixed, hot plasma is advected around the companion and lines the inner surface of the hole. Therefore, it will also contribute to the overall burst emission. For completeness, we would like to mention that both the unshocked ejecta and the unshocked envelope will be irradiated by the corresponding shocked material lying across the contact discontinuity. The irradiating components will only be partially reflected with the majority of X-ray photons down-scattered to lower energies (see, e.g., Plewa 1995).

Although we are not in a position to predict the actual contribution to the emission from the companion (the mixed material or effects due to irradiation), our simulation results provide information about the amount of the energy deposited by shocks in the ejecta and the envelope, along with their corresponding characteristic temperatures. By comparing the characteristics of the shock-heated envelope to those of the shock-heated ejecta, combined with the semi-analytic predictions by Kasen (2010), we can provide upper limits for the contribution of the shock-heated envelope material to the flash emission. We note that the results of our hydro simulations contain all of the information required to perform realistic radiation transport calculations of the prompt emission. Such calculations are, however, beyond the scope of the present study. Here we first consider the ejecta material heated by the reflected shock, which is created when the forward supernova shock penetrates into the companion's envelope. Then we discuss the properties of the shocked stellar envelope.

Fig. 10 shows the internal energy distributions as a function of temperature for our selected subset of model binary systems for the ejecta (left panel) and the stellar envelope (right panel). The energy distributions are shown at the simulation time,  $t = t_h$ , when the increase of the internal energy due to shock heating is at its maximum value. To estimate the amount of energy deposited by the reflected shock (in the ejecta), we calculated the internal energy of the ejecta material above and below the mid-plane of the computational domain,  $z = 0$  cm, corresponding to the vertical position of

the explosion center. The difference between the internal energies of the ejecta material in those two regions is equal to the energy produced by heating due to the reflected shock. As for the heating of the stellar envelope, the amount of internal energy deposited by the transmitted shock can be found by simply subtracting the internal energy of the stellar material at a given time from the initial internal energy of the envelope.

A number of comments regarding the distributions of internal energy shown in Fig. 10 are in order. The effects of heating by the reflected shock are the strongest in the case of the MS38 model for temperatures between  $T \approx 6 \times 10^6$  K and  $T \approx 7 \times 10^7$  K. No internal energy is seen at the initial time in this model (shown with a thin solid line in the left panel of Fig. 10) in this range of temperatures. The reflected shock is also capable of producing a substantial amount of high-temperature ( $T > 1 \times 10^8$  K) shocked ejecta, but only in the case of low-density RG companion (shown with a thick dashed line in the left panel of Fig. 10). The material located at temperatures greater than approximately  $1 \times 10^8$  K and below  $3 \times 10^8$  K are the ejecta that swept around the companion shown in Fig. 2(a). The ejecta material present at still higher temperatures corresponds to the supernova's forward and reverse post-shock regions (and is largely unaffected by the interaction with the companion).

In the case of the heated companion material (shown in the right panel in Fig. 10), the strongest heating occurs in the MS38 and SG models, while the RG experiences relatively weaker heating and to lower temperatures. However, it is the RG's envelope that experiences the relatively greatest amount of shock heating at temperatures above  $1 \times 10^8$  K. This hot companion material is associated with the conical shock that develops along the center line of the ejecta hole (cf. Section 3.1). The properties of this material are somewhat uncertain given the assumed symmetry in our simulations.

Table 3 summarizes the characteristics of the energy deposited by the transmitted and reflected shocks. In particular, the table provides information about the residual, shock-deposited internal energy in the ejecta and the envelope,  $e_{r,48}$ , and the internal energy-weighted, characteristic temperature of the residual internal energy,  $T_r$ . We note that the shock heating of the companion's envelope produces comparable amounts of internal energy to that of the heating of the ejecta by the reflected shock. The reflected shock produces between 10 per cent more energy than the transmitted shock in the case of the MS38 system and 50 per cent in the case of the RG319 system. This implies that the thermalization process of the explosion energy is more efficient for dense, compact companions. Also, the characteristic temperatures of the energy deposited by the transmitted shock are higher in the case of such compact companions. Consequently, the spectra produced by those shocks will be somewhat harder than the emission of corresponding reflected shocks. Assuming the radiating plasma is in thermal equilibrium, the characteristic temperatures of the shock-heated ejecta material produced in the process of the supernova-companion interaction correspond to soft X-ray emission with typical energies around 3.8, 1.8, and 0.14 keV in the case of MS, SG, and RG companions, respectively.

The amount of the residual internal energy of the ejecta produced in our models is by a factor of about 2.6–4.3 lower

<sup>1</sup> As pointed out by Kasen (2010), the emission produced by this material has the best chance of being observed at early times. This is because, and in contrast to the shock-heated envelope, it remains unobscured by the dense ejecta when viewed at angles for which the opacity is sufficiently small. Such low opacities at early times can only be found for viewing angles inside the ejecta hole.

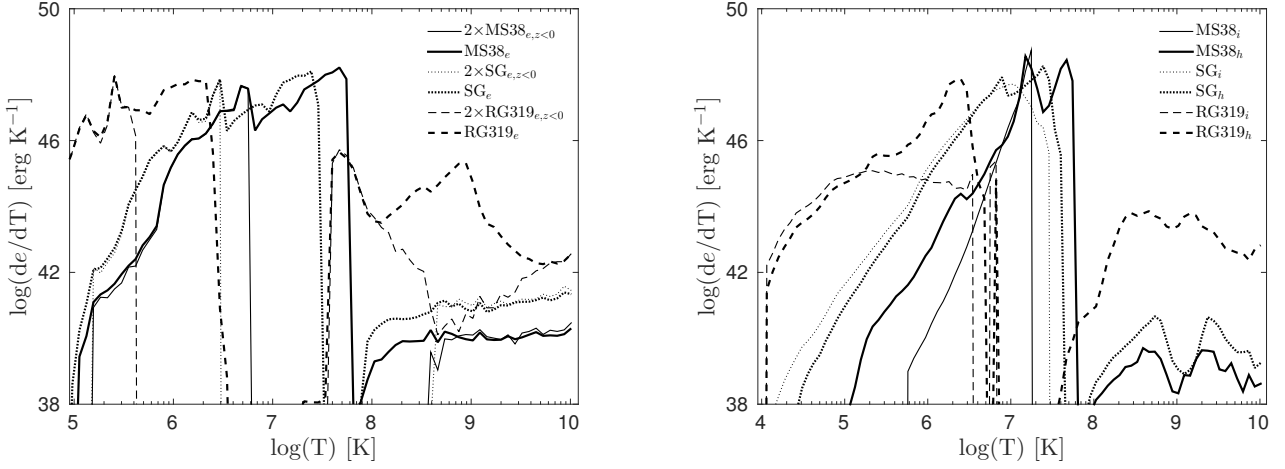


**Figure 10.** Temperature distribution of internal energy for a subset of our model binary systems. For both panels, the MS model MS38 is shown with a solid line, the subgiant SG is shown with a dotted line, and the red giant RG319 is shown with a dashed line. In the left panel, the supernova ejecta internal energy is shown at the time when the increase in the ejecta’s internal energy is near its highest point,  $t_h$ . Here the thin lines correspond to the ejecta material largely unaffected by interaction with the companion (twice the amount of the ejecta internal energy located in the lower half of the computational domain), while the thick lines correspond to the whole ejecta material. The right panel shows the bound and unbound companion material at the initial time,  $t_i$  (thin lines), and at  $t_h$  (thick lines), with  $t_h$  defined as for the left panel. Note that the temperature is shown in log scale; see text for discussion.

**Table 3.** Residual internal energy,  $e_{r,48}^a$ , and characteristic, energy-weighted temperature of the residual internal energy,  $T_r$ , for the supernova ejecta and companion material for a subset of our binary models.

Model	Ejecta		Envelope	
	$e_{r,48}$ [erg]	$T_r$ [keV]	$e_{r,48}$ [erg]	$T_r$ [keV]
MS38	6.6	3.8	5.9	4.1
SG	5.3	1.8	4.0	2.2
RG319	4.0	0.14	2.6	0.21

<sup>a</sup> The residual internal energy,  $e_{r,48}$ , is given in the units of  $10^{48}$  erg.

than the semi-analytic estimate of the collision energy, provided by Kasen (2010), of about  $1.7 \times 10^{49}$  erg (using equation 11 in Kasen (2010) for the explosion energy of our supernova model). After taking into account the energy deposited in the envelope, these factors decrease to about 1.4 and 4.1. Because the contribution of the shocked envelope to the prompt emission will likely be lower than its estimated residual internal energy, our estimates provide upper limits for the energy available to the flash.

Kasen’s estimates of the typical energies of the prompt emission are in good agreement with our estimates of the characteristic, energy-weighted temperatures of the shock-heated material in the case of the RG model companion. Our MS model, however, produces shocked plasmas with temperatures higher than those predicted by Kasen by a factor of about 2. In passing, we note that admixture of the stripped, shock-heated envelope material will make the emitted spectrum somewhat harder compared to the spectrum of the emission radiated by the shocked ejecta alone.

Marion et al. (2016) applied Kasen’s model to observations of SN 2012cg, and found the best agreement with his  $6 M_{\odot}$  model. Because it is very unlikely that a  $6 M_{\odot}$

MS star can be a binary companion of a Chandrasekhar-mass white dwarf, we attempted to identify a binary system with characteristics most closely matching the 6 solar mass system of Kasen among our sample. The orbital distance of Kasen’s  $6 M_{\odot}$  model,  $a \approx 29 R_{\odot}$ , places that system between our SG and RG319 models. Additionally, his estimate of the characteristic temperature of the prompt emission of 0.2 keV matches the characteristics of our RG319 system most closely (especially if the contribution of the shocked envelope is taken into account; the SG emission is much harder with a characteristic temperature of about 2 keV). We conclude that the most likely companion of the SN 2012cg system was a post-MS, possibly transiting to become a RG star.

#### 4.7 Numerical resolution effects

The interaction between the supernova ejecta and the companion produces flow features and involves phenomena that put the simulation codes used to study this process to the test. On the one hand, the simulation code must maintain a stellar companion in hydrostatic equilibrium for several sound crossing times of the stellar envelope. On the other

hand, the code has to correctly capture the fast-moving supernova shock, its interaction with the companion's envelope, in particular heating of the envelope and the formation and evolution of the reflected shock. Furthermore, the presence of shear between the supernova ejecta and the companion's envelope induces Kelvin-Helmholtz instability (KHI) and mixing, and contributes to the process of stripping outer layers from the companion.

The use of an adaptive mesh refinement method, along with the high-resolution shock capturing hydrodynamic method offered two ways of controlling the quality of the numerical solution. First, the mesh was refined in the regions containing substantial gradients of density and pressure. This allows for capturing flow discontinuities such as shocks and the KHI-unstable material interfaces that are the most affected by numerical diffusion. Second, by changing the effective mesh resolution in those regions we were able to control the actual amount of numerical diffusion in the solution and thus its quality. From the point of view of the current application, the numerical diffusion will affect model predictions such as the amount of stripped mass, contamination of the companion with the ejecta material, and structure of the ejecta hole.

To assess the impact of numerical diffusion on the model observables in our simulations, we performed a series of numerical experiments varying the effective mesh resolution. Fig. 11 shows the amount of stripped material as a function of time for our basic set of binary models. For each binary type, the results are shown in two sub-panels. In the first sub-panel we show the evolution of stripped mass during the early, most violent, phase of the interaction, while in the second sub-panel we show the amounts of stripped mass at late times until the final simulated time. In all models, the amount of stripped mass increases rapidly as the ejecta shears over the shocked envelope material, and begins to level off around the time when the transmitted shock reaches the core of the companion, the bound stellar material starts to expand, and mass stripping becomes dominated by the vorticity deposited by the supernova shock in the surface layers of the companion. The numerical effects appear to most strongly affect the SG (middle panel in Fig. 11) during that later phase as compared to the main sequence MS38 model (left panel in Fig. 11). This is most likely due to a shallower density gradient in the envelope of the SG that allows for a relatively greater deposition of the vorticity in its envelope. Because the vorticity generation process involves interaction between the gradients of density and pressure, this process thus sensitively depends on numerical resolution.

The amount of stripped mass may decrease or increase with the resolution, and this behavior clearly depends on the companion type. For example, the amount of stripped mass increases with resolution in the case of a MS star (right subpanel in the left-hand panel of Fig. 11), while it decreases for the RG model (right subpanel in the right-hand panel in Fig. 11). The behavior in the case of the SG is similar to that of the RG companion, but the convergence is slower.

Overall, the amount of stripped mass found in the L100 and L200 models does not differ by more than about 5 per cent, which is found in the case of the SG model. The supernova-companion interaction problem shares several similarities with the shock-cloud interaction problem.

The latter has been extensively studied by means of multi-dimensional hydrodynamic and magnetohydrodynamic simulations. The original work by Klein et al. (1994) considered the hydrodynamics of shock-cloud interaction, and Mac Low et al. (1994) extended the model problem to magnetohydrodynamics. These groups found that a resolution of at least 100 mesh cells per cloud radius was necessary in order to correctly capture the dynamics of the shock-cloud interaction in terms of the overall cloud shape, its integrated parameters (e.g. average density), and the cloud destruction time. This conclusion was later confirmed by Shin et al. (2008) in three dimensions. In the context of the present application, the original work by Marietta et al. (2000) used a resolution of approximately 125 zones per companion radius, and found the amount and average dynamics of the stripped material converged at the level of about 6 per cent. A similar accuracy of about 8 per cent was found in the more recent three-dimensional study by Pan et al. (2012a), who used about 70 cells per companion radius. (A comparable accuracy in studies using an SPH technique required at least 500,000 particles per stellar companion (Pakmor et al. 2008).) The estimated error of at most 5 per cent found in our L200 models is therefore consistent with the results of convergence studies performed by these groups.

It is important to mention that the convergence in terms of the amount of stripped mass does not guarantee convergence in other quantities, and likely depends on the specific characteristics of the computational model employed. In particular, Pakmor et al. (2008) anticipated slower convergence in terms of mixing between the ejecta and stellar companion material due to a relatively poor performance of SPH in resolving hydrodynamic instabilities. Also, one needs to be particularly careful with predictions that involve relatively small amounts of mass. The prime example here is the contamination of the companion with the heavy elements produced by the supernova. Pan et al. (2012a) found the maximum contamination levels of  $10^{-4} M_{\odot}$  in the case of their compact helium star. This has to be compared to the highest contamination result of  $10^{-7} M_{\odot}$  in the case of our SG. Because mesh-based, Eulerian methods are prone to produce artificial mixing of materials, it is conceivable that these predictions are subject to strong numerical diffusion effects. For example, we found that the amount of contamination decreases with resolution for our main sequence MS38 model by a factor of 13 when the resolution is increased from L50 to L100, and by another factor of 1.6 when the resolution is increased from L100 to L200. In the case of our SG model, the level of contamination decreases by a factor of about 27 when the resolution is increased from L50 to L100, and by about 35 per cent as the resolution is increased from L100 to L200. Clearly, more careful error estimation studies are required when one wants to predict accurate levels of contamination.

We found that the amounts of energy stored by both the reflected shock in the ejecta and the transmitted shock in the envelope depend only relatively weakly on the numerical model resolution. Specifically, the amount of energy stored by the reflected shock in the ejecta varies by no more than 2 per cent as the resolution increases from L100 to L200. The convergence of the energy stored by the transmitted shock in the companion's envelope is slowest in the case of the RG model, with the residual energy decreasing by about 8 per

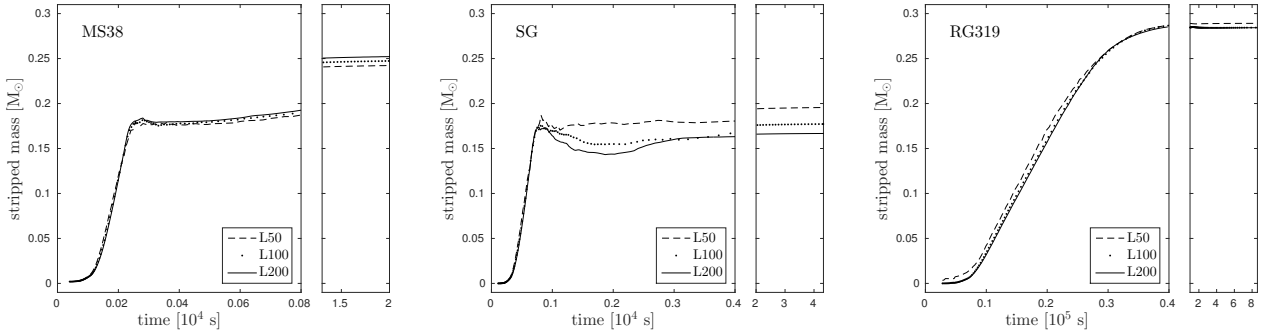


**Figure 11.** Volume-integrated stripped companion mass as a function of time for a subset of model binary systems. (left panel) the main sequence model MS38; (middle panel) the subgiant SG; (right panel) the red giant RG319. Each panel is split into two sub-panels to show the initial behavior (left sub-panels) and the late-time behavior (right sub-panels). The stripped mass is shown with dashed, dotted, and solid lines for models with effective mesh resolutions of L50, L100, and L200 cells per companion radius, respectively. Note a relatively slow convergence in the amount of stripped mass in the SG case.

cent as the resolution is increased to 200 cells per companion radius. However, the convergence is much faster in the case of more compact companions. Also, we did not find a substantial dependence of the average temperature of the residual energy on the mesh resolution in our simulations.

## 5 SUMMARY AND CONCLUSIONS

We have studied the interaction between an exploding Chandrasekhar-mass white dwarf with its non-degenerate companion by means of high-resolution, hydrodynamical simulations in two dimensions, neglecting the effects of orbital motion or spin of the companion. We followed the evolution for a set of realistic binary system models with MS, SG, and RG companions.

For each model binary system, we obtained a series of simulations with progressively increasing mesh resolution in order to assess numerical model convergence. We presented details of simulations for a representative subset of our model binary systems. We discussed evolution and morphology of the exploding supernova ejecta, kinematic properties of material stripped from companion stars, and possible contamination of companions with the the metal-rich ejecta material. We discussed, for the first time, the amount and thermal characteristics of the dense, X-ray emitting layers of the stellar envelope and the ejecta heated by the shocks created in the process of interaction of the supernova shock with the stellar envelope.

Our main findings can be summarized as follows.

- (i) We found that the supernova interaction with the stellar companion affects the entire hemisphere of the ejecta facing the companion. The ejecta structure is most strongly affected in the part which directly impacts the companion. The visible effect of this interaction is the ejecta hole, a conically-shaped region extending behind the companion. The typical half-opening angle of the ejecta hole found in our simulations varied between 40 and 50 degrees. These results are in good agreement with the findings reported by other groups.
- (ii) We found the amount of mass stripped from a stellar companion to depend on the companion class. The envelopes of

both of our RG model companions were completely stripped off, the finding consistent with the results of other groups, with both stars losing about 40 per cent of their initial mass. The least amount of stripped mass was found in the case of the SG companion, which lost only about 10 per cent of its initial mass.

- (iii) The MS companion models produced mass loss in good agreement with the power-law relation between stripped mass and orbital separation of Pakmor et al. (2008). These companions typically lost about a quarter of their initial mass, which is generally greater than the mass loss reported by other groups (our results match the predictions of Pan et al. 2012a most closely).
- (iv) We analyzed kinematic properties of the stripped companion material, and found the stripped material to move with characteristic speeds between 500 and 700 km s<sup>-1</sup>. These characteristic speeds are uniformly lower than the values presented by Marietta et al. (2000), presumably due to the lower energy of the supernova explosion used in our study. The numerical effects may also contribute to the observed discrepancy. Lower model mesh resolution and a different analysis method may explain much higher peak velocities of the stripped companion material reported by Pan et al. (2012a). However, there is a good qualitative agreement between their velocity distributions of the stellar material and our results.
- (v) We found about 10<sup>-4</sup> M<sub>⊙</sub> of hydrogen moving with speeds above 13 000 km s<sup>-1</sup> in our subset of model binary systems. The greatest amount of fast-moving hydrogen is produced in the case of the SG model, while the least amount is found in the case of RG companions. Additionally, the fastest moving hydrogen is found in the case of the SG companion, while the slowest hydrogen is produced in the process of interaction with the supernova with red giants. This correlation between the amount and speed of stripped hydrogen holds for all classes of companions also at lower velocities, contrary to the predictions of Marietta et al. (2000). Therefore, and as originally suggested by Marietta et al., observations of hydrogen in early Type Ia spectra may indeed help identification of stellar companion classes.
- (vi) Our model companion stars were polluted with only small amounts of the ejecta material. We found the highest levels



of  $Ni^{56}$  enrichment of  $\approx 10^{-7} M_{\odot}$  in the case of the SG model. Such low levels of contamination can be attributed to the assumed model symmetry and reduced dimensionality that prevented us from including the effects of orbital motion and companion's spin (see, e.g., [Pan et al. 2012a](#)).

- (vii) We carefully analyzed and, for the first time, provided simulation-based estimates of the amounts and of the thermal characteristics of the shock-heated plasma expected to produce a flash of soft X-ray radiation during early phases of the supernova-companion interaction. We found the overall good qualitative agreement with estimates of the semi-analytic model of [Kasen \(2010\)](#). However, our models predict the energy budget available for the prompt emission by a factor 2–4 smaller, even though we also account for the energy deposited in the companion's envelope by the transmitted supernova shock. These numerical estimates of the amounts of residual energy appear to be accurate to within a few per cent in our models.
- (viii) We estimated characteristic temperatures of the shocked ejecta material of 0.14 and 1.8 keV in the case of a RG and MS companion, respectively, in good agreement with the Kasen's model. In addition, we predict the SG model to produce the hardest X-ray emission of the shocked ejecta with average temperatures of nearly 4 keV. These results appear very weakly dependent on numerical model resolution in our simulations.
- (ix) We also analyzed properties of the shock-heated envelope material of stellar companions. Although this material was not included in the Kasen's model, we predict that it will directly contribute to the prompt emission as it is transported along the inner surface of the ejecta hole and mixes with the shocked ejecta. The amount of the energy deposited in the envelope by the transmitted supernova shock is comparable to the energy stored by the reflected shock in the ejecta, while its characteristic temperatures are somewhat higher. The latter property implies the spectrum of the flash produced by both post-shock regions will be somewhat harder than the spectrum emitted by the shocked ejecta alone.
- (x) The plasma produced by shocks across the contact discontinuity will irradiate the material located across the contact surface. This soft X-ray emission will only be partially reflected with the majority of photons scattered down to lower energies (see, e.g., [Plewa 1995](#)). As a result, a softer component will be added to the shock-dominated prompt emission spectrum.
- (xi) Chemical pollution of the companion star proved particularly sensitive to numerical diffusion effects. For example, in the case of our MS and SG models, the contamination of the companion star increased by 60 and 35 per cent, respectively, after we doubled the mesh resolution to 200 cells per stellar radius. This strongly suggests that accurate predictions of the companion's chemical enrichment may require simulations with 200 or more cells per companion's radius. The amount of stripped material appears less dependent on mesh resolution, and converges with accuracy better than about 10 per cent in models with 200 cells per stellar radius.

Future research should focus on obtaining numerically converged, three-dimensional models of the supernova-companion interaction to provide reliable estimates of the stripped mass, especially in the case of MS and SG compan-

ions. Evolved for sufficiently long times, such models would also help to better understand the process of pollution of companion stars with metal-rich ejecta material. Models of the prompt emission should consider the energy budget that takes into account the shocked ejecta as well as the shocked envelope material, which is advected along the inner surface of the ejecta hole and mixed with the ejecta.

## ACKNOWLEDGMENTS

TP was partially supported by the NSF grant AST-1109113 and the DOE grant DE-SC0008823. This research used resources of the National Energy Research Scientific Computing Center, which is supported by the Office of Science of the U.S. Department of Energy under Contract No. DE-AC02-05CH11231. The software used in this work was in part developed by the DOE Flash Center at the University of Chicago. The data analysis was performed in part using MATLAB<sup>®</sup> ([Mathworks 2015](#)), and VisIt ([Childs et al. 2012](#)). This research has made use of NASA's Astrophysics Data System Bibliographic Services.

## REFERENCES

- Branch D., Tammann G. A., 1992, [ARA&A](#), **30**, 359
- Cao Y., et al., 2015, [Nature](#), **521**, 328
- Childs H., et al., 2012, in , High Performance Visualization—Enabling Extreme-Scale Scientific Insight. pp 357–372
- Colella P., Woodward P. R., 1984, [J. Comput. Phys.](#), **54**, 174
- Fryxell B., et al., 2000, [ApJS](#), **131**, 273
- García-Senz D., Badenes C., Serichol N., 2012, [ApJ](#), **745**, 75
- Hayes W. D., Probst R. F., 2004, *Hypersonic Inviscid Flow*. Dover, New York
- Hillebrandt W., Niemeyer J. C., 2000, [ARA&A](#), **38**, 191
- Iben Jr. I., Tutukov A. V., 1984, [ApJS](#), **54**, 335
- Ivanova N., Taam R. E., 2004, [ApJ](#), **601**, 1058
- Kasen D., 2010, [ApJ](#), **708**, 1025
- Klein R. I., McKee C. F., Colella P., 1994, [ApJ](#), **420**, 213
- Langer N., Deutschmann A., Wellstein S., Höflich P., 2000, [A&A](#), **362**, 1046
- Liu Z. W., Pakmor R., Röpke F. K., Edelmann P., Wang B., Kromer M., Hillebrandt W., Han Z. W., 2012, [A&A](#), **548**, A2
- Liu Z.-W., Pakmor R., Röpke F. K., Edelmann P., Hillebrandt W., Kerzendorf W. E., Wang B., Han Z. W., 2013a, [A&A](#), **554**, A109
- Liu Z.-W., et al., 2013b, [ApJ](#), **774**, 37
- Mac Low M.-M., McKee C. F., Klein R. I., Stone J. M., Norman M. L., 1994, [ApJ](#), **433**, 757
- Marietta E., Burrows A., Fryxell B., 2000, [ApJS](#), **128**, 615
- Marion G. H., et al., 2016, [ApJ](#), **820**, 92
- Mathworks T., 2015, version 8.5.0.197613 (R2015a). The MathWorks Inc., Natick, Massachusetts
- Nomoto K., 1982, [ApJ](#), **253**, 798
- Nomoto K., Thielemann F.-K., Yokoi K., 1984, [ApJ](#), **286**, 644
- Pakmor R., Röpke F. K., Weiss A., Hillebrandt W., 2008, [A&A](#), **489**, 943
- Pan K.-C., Ricker P. M., Taam R. E., 2010, [ApJ](#), **715**, 78
- Pan K.-C., Ricker P. M., Taam R. E., 2012a, [ApJ](#), **750**, 151
- Pan K.-C., Ricker P. M., Taam R. E., 2012b, [ApJ](#), **760**, 21
- Pan K.-C., Ricker P. M., Taam R. E., 2013, [ApJ](#), **773**, 49
- Pan K.-C., Ricker P. M., Taam R. E., 2014, [ApJ](#), **792**, 71
- Phillips M. M., 1993, [ApJ](#), **413**, L105
- Plewa T., 1995, [MNRAS](#), **275**, 143
- Ruiz-Lapuente P., 2014, [New Astron. Rev.](#), **62**, 15
- Ruiz-Lapuente P., et al., 2004, [Nature](#), **431**, 1069

- Shin M.-S., Stone J. M., Snyder G. F., 2008, [ApJ](#), **680**, 336
- Timmes F. X., Swesty F. D., 2000, [ApJS](#), **126**, 501
- Webbink R. F., 1984, [ApJ](#), **277**, 355
- Whelan J., Iben Jr. I., 1973, [ApJ](#), **186**, 1007
- Williams B. J., Chomiuk L., Hewitt J. W., Blondin J. M., Borkowski K. J., Ghavamian P., Petre R., Reynolds S. P., 2016, [ApJ](#), **823**, L32
- Xue Z., Schaefer B. E., 2015, [ApJ](#), **809**, 183
- Zhou P., Chen Y., Zhang Z.-Y., Li X.-D., Safi-Harb S., Zhou X., Zhang X., 2016, preprint, ([arXiv:1605.01284](#))
- van Dyke M., 1982, *An album of fluid motion*. Stanford: Parabolic Press